Robotics and Autonomous Systems 62 (2014) 1486–1496

Contents lists available at ScienceDirect

Robotics and Autonomous Systems

journal homepage: www.elsevier.com/locate/robot

Homography estimation from circular motion for use in visual control

Andrej Zdešar *, Igor Škrjanc, Gregor Klančar

Laboratory of Autonomous Mobile Systems, Faculty of Electrical Engineering, Tržaška 25, 1000 Ljubljana, Slovenia

HIGHLIGHTS

- Only one point rotating at constant velocity around a single axis is required.
- The proposed method estimates the homography and the angular velocity of the rotating point.
- All the measurements required in the estimation can be obtained in the image.

ARTICLE INFO

Article history:
Received 8 May 2013
Received in revised form
26 January 2014
Accepted 26 May 2014
Available online 2 June 2014

Keywords:
Camera calibration
Circular points
Conic section
Homography

ABSTRACT

This paper presents a new method for estimation of the homography up to similarity from observing a single point that is rotating at constant velocity around a single axis. The benefit of the proposed estimation approach is that it does not require measurement of the points in the world frame. The homography is estimated based on the known shape of the motion and in-image tracking of a single rotating point. The proposed method is compared to the two known methods: the direct approach based on point correspondences and a more recently proposed method based on conic properties. The main advantages of the proposed method are that it also estimates the angular velocity and that it requires only a single circle. The estimation is made directly from the measurements in the image. Because of the advantages of the proposed method over the other methods, the proposed method should be simple to implement for calibration of visually guided robotic systems.

All the approaches were compared in the simulation environment in some non-ideal conditions and in the presence of disturbances, and a real experiment was made on a mobile robot. The experimental results confirm that the presented approach gives accurate results, even in some non-ideal conditions.

1. Introduction

Camera calibration is one of the fundamental tasks in computer vision. Results of many computer vision algorithms depend on good camera calibration, e.g. image rectification, 3D reconstruction, visual servoing, etc. The problem of camera calibration has been addressed by many authors, and the topic is normally addressed in every computer vision book, e.g. [1]. The conventional calibration approaches normally require a special preparation of the working environment, usually by insertion of an object with known dimensions into the environment, like a chessboard pattern [2–4], a pattern of circular markers [5], or other conic patterns [6–10], etc. Different calibration procedures use different camera models that give different accuracies. Normally it suffices to use only a basic pinhole camera model, but this model gives inaccurate results in presence of large lens distortions, so a more general model must be considered [4,11]. The applicability of a particular method depends on the environment in which the method is to be used.

The conventional calibration techniques [2] are based on estimation of the camera model from a set of non-coplanar world points and their images using the least squares or some other minimization algorithm, and decomposition of the estimated model (normally in matrix form) into the camera intrinsic and extrinsic parameters. Zhang [3] proposed a similar approach that is also based on decomposition, but from a set of homography matrices. This work focuses on estimation of the *homography*, a transformation that relates two planes under perspective projection. In computer vision, a homography is normally used to describe the relation between two image planes, an image plane and a world plane or two world planes. There exist well known algorithms for extraction of the camera intrinsic and extrinsic parameters from multiple homographies that all relate to the same image plane [3]. In this paper we investigate several homography estimation techniques that can easily be deployed in visually guided robotic

* Corresponding author. Tel.: +386 14768950.
E-mail addresses: andrej.zdesar@fe.uni-lj.si (A. Zdešar), igor.skrjanc@fe.uni-lj.si (I. Škrjanc), gregor.klancar@fe.uni-lj.si (G. Klančar).

http://dx.doi.org/10.1016/j.robot.2014.05.012
0921-8890/

systems. The basic idea is to use robot motion in order to eliminate the need for special preparation of the environment solely for the purpose of camera calibration.

Recently, many approaches for camera calibration that are based on studying the invariance of the conics under perspective transformation have been proposed. Sugimoto [6] presented the estimation from seven corresponding conics by solving an over constrained algebraic set of equations. It has been shown that at the minimum a pair of conic correspondences is needed for estimation [7]. Many authors studied different configurations of conics: coplanar circles [9,10], lines intersecting the circle centre [12], concentric circles [13], etc.

Wong [14] studied self calibration from axial symmetric objects (*surfaces of revolution*), objects that are frequently found in man-made environments and have some special structure, but the exact geometry is not known. In this paper we present a calibration procedure for estimation of the homography up to similarity that is based on circular motion of some world point around the single axis. The method for camera calibration and 3D reconstruction from rotation of an object about a single axis was shown in [15,16]. The approach [15] requires image tracking of several points in the rotating object. The method presented in this paper requires image tracking of only a single point, but it requires constant angular velocity, which is not required for the use of [15].

Provided that camera intrinsic parameters are known, orientation and position of the camera with respect to the ground plane can be determined [17]. In visual control, pose of the camera (object) with respect to some ground plane is a valuable piece of information that can be used to improve autonomy of many robotic tasks, like automatic landing of air-planes [18], hovering and navigation of helicopters or quadrocopters [19], etc. Once the transformation between the image and ground plane (homography) is established, a view from a virtual camera looking perpendicular to the ground plane can be obtained. The homography can be used directly in visual control of mobile robots [20–22].

This paper is structured as follows. In Section 2 an overview of the basic projective transformation relations is given and conventional methods for camera calibration are presented. Section 3 presents three different methods for homography estimation from circular motion. In Section 4 the results of the experimental validation are presented and comparison of the methods is given. Afterwards, a discussion of the results is given in Section 5 and in the final section, Section 6, some conclusions are drawn.

2. Calibration overview

2.1. Points, lines and conics under perspective projection

If not specified differently, small bold-face letters (e.g. $\boldsymbol{x}$) are used to denote column vectors (e.g. homogeneous points) and big bold-face letters (e.g. $\boldsymbol{X}$) for matrices. The subscript $(\cdot)_w$ is used to denote the world coordinate frame, $(\cdot)_p$ for the picture (image) frame and $(\cdot)_c$ for the camera frame.

The transformation between the point $\boldsymbol{p}_w^T = [x_w\ y_w\ z_w\ 1]$ in the world frame and the corresponding point $\boldsymbol{p}_p^T = [x_p\ y_p\ 1]$ in the image frame can be described by a pinhole camera model [23]:

$$w\boldsymbol{p}_p = \boldsymbol{S}\begin{bmatrix}\boldsymbol{R} & \boldsymbol{t}\end{bmatrix}\boldsymbol{p}_w, \quad \boldsymbol{S} = \begin{bmatrix}\alpha & \gamma & x_{pc}\\ 0 & \beta & y_{pc}\\ 0 & 0 & 1\end{bmatrix}, \tag{1}$$

where w is a scalar weight, while the matrix $\boldsymbol{R} \in \mathbb{R}^3 \times \mathbb{R}^3$ and the vector $\boldsymbol{t} \in \mathbb{R}^3$ describe camera orientation and position with respect to the world frame. The upper-triangular matrix $\boldsymbol{S}$ contains the intrinsic camera parameters: the scaling factors α and β in horizontal and vertical direction, respectively; the optical axis centre (x_{pc}, y_{pc}) and the skew factor γ. The model (1) is non-linear because of the dependence $w = w(\boldsymbol{p}_w)$.

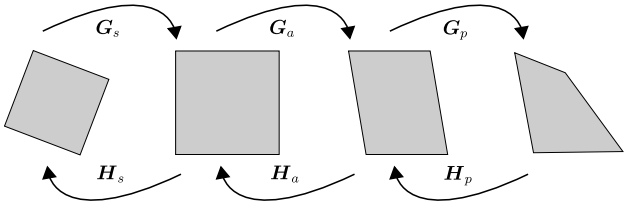

Fig. 1. Effects of all three basic transformations on a square: first to second, similarity; second to third, affine; and third to last, pure projective transformation.

If the world points are confined to a common plane, the relation (1) simplifies. Without loss of generality, assume that the image plane spans the axis vectors x_w and y_w ($z_w = 0$):

$$w\boldsymbol{p}_p = \boldsymbol{S}\begin{bmatrix}\boldsymbol{r}_1 & \boldsymbol{r}_2 & \boldsymbol{t}\end{bmatrix}\begin{bmatrix}x_w\\ y_w\\ 1\end{bmatrix} = \boldsymbol{G}\boldsymbol{p}_w\,, \tag{2}$$

where the vector $\boldsymbol{p}_w^T = [x_w\ y_w\ 1]$ has been redefined. In machine vision community, the matrix $\boldsymbol{G} \in \mathbb{R}^3 \times \mathbb{R}^3$ is known as *homography*. Denoting $\boldsymbol{G}^T = [\boldsymbol{g}_1\ \boldsymbol{g}_2\ \boldsymbol{g}_3]$, from Eq. (2) follows:

$$x_p = \frac{\boldsymbol{g}_1^T\boldsymbol{p}_w}{\boldsymbol{g}_3^T\boldsymbol{p}_w} \quad \text{and} \quad y_p = \frac{\boldsymbol{g}_2^T\boldsymbol{p}_w}{\boldsymbol{g}_3^T\boldsymbol{p}_w}. \tag{3}$$

For the sake of notation simplicity, a new symbol for the inverse of the homography is introduced: $\boldsymbol{H} = \boldsymbol{G}^{-1}$. The inverse homography mapping $\boldsymbol{H}$ can be decomposed into a set of elementary transformations known as similarity, affine and pure projective transformation:

$$\boldsymbol{H} = \underbrace{\begin{bmatrix}s\cos\varphi & -s\sin\varphi & t_x\\ s\sin\varphi & s\cos\varphi & t_y\\ 0 & 0 & 1\end{bmatrix}}_{\boldsymbol{H}_s}\underbrace{\begin{bmatrix}\frac{1}{b} & -\frac{a}{b} & 0\\ 0 & 1 & 0\\ 0 & 0 & 1\end{bmatrix}}_{\boldsymbol{H}_a}\underbrace{\begin{bmatrix}1 & 0 & 0\\ 0 & 1 & 0\\ l_1 & l_2 & l_3\end{bmatrix}}_{\boldsymbol{H}_p}. \tag{4}$$

The transformation $\boldsymbol{H}_p$ maps points from the image space to the affine space, the transformation $\boldsymbol{H}_a$ from the affine to the metric space and the matrix $\boldsymbol{H}_s$ from the metric to Euclidean space. The effects of all three elementary transformations on a square can be observed in Fig. 1. In the similarity matrix, the element s describes the scaling factor, the tuple (t_x, t_y) translation and the angle φ right-handed planar rotation (around the axis z). The parameters a and b of the affine to metric transformation define the shrinkage and skewness. The last row in the pure projective transformation matrix $\boldsymbol{H}_p$ contains the parameters of the vanishing line of the observed plane $\boldsymbol{l}_{p\infty}^T = [l_1\ l_2\ l_3]$.

Lines are invariant under projective transformation, in other words, lines transform into lines: $\boldsymbol{l}_p = \boldsymbol{H}^T\boldsymbol{l}_w$. More generally, conic sections (conics) remain conics under projective transformation. The equation of a general conic in the implicit form is as follows:

$$\boldsymbol{p}_w^T\boldsymbol{C}_w\boldsymbol{p}_w = 0, \quad \boldsymbol{C}_w = \begin{bmatrix}A & B/2 & D/2\\ B/2 & C & E/2\\ D/2 & E/2 & F\end{bmatrix}, \tag{5}$$

where all the parameters of the conic are gathered in the symmetric matrix $\boldsymbol{C}_w$. Substituting $\boldsymbol{p}_w$ for (2) gives the solution to the description of the corresponding conic in the image frame $\boldsymbol{p}_p^T\boldsymbol{C}_p\boldsymbol{p}_p = 0$:

$$\boldsymbol{C}_p = \boldsymbol{H}^T\boldsymbol{C}_w\boldsymbol{H}. \tag{6}$$

Another property of interest is the relation between the angle in the image frame φ_p and the corresponding angle in the world plane

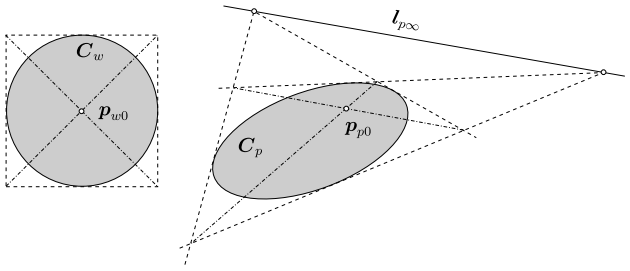

Fig. 2. Transformation of a circle and parallel lines from the world plane (left) to the image plane (right).

φ_w. The relation can be obtained from differentiation of Eq. (2). Taking into account $\boldsymbol{g}_3^T \boldsymbol{H} \boldsymbol{p}_p = 1$, after some algebraic manipulation, the following equation can be obtained:

$$\tan \varphi_w = \frac{(g_{21} - y_p g_{31}) \cos \varphi_p - (g_{11} - x_p g_{31}) \sin \varphi_p}{(g_{12} - x_p g_{32}) \sin \varphi_p - (g_{22} - y_p g_{32}) \cos \varphi_p}. \tag{7}$$

Note that this relation is dependent on the image coordinates $\boldsymbol{p}_p$.

To estimate all the intrinsic parameters in $\boldsymbol{S}$, Zhang's approach [3] requires three or more homographies that relate the non-parallel planes to the image frame. Including some a-priori knowledge about the camera parameters the approach can be used to estimate the camera parameters even from two (e.g. assuming no image skew $\gamma = 0$) or only one homography (e.g. already known parameters need not be estimated). However, the first step in recovering the camera parameters is estimation of the homography matrices.

In some cases, the estimation of all the intrinsic parameters may not even be needed. Often we are only interested in obtaining the homography up to similarity, which means that we are interested only in the matrix $\boldsymbol{H}_a \boldsymbol{H}_p$ — the transformation is also known as metric rectification, since it enables us to remove the projective distortion with respect to the world plane. As an illustration, consider the problem of visual control of a mobile robot from an overhead camera. To simplify the control design, the canonical configuration is considered whenever possible, where the camera is placed in a way that the image plane is parallel to the ground plane in which the robot is moving [24]. In a more general case where the camera is placed at an arbitrary inclination with respect to the ground plane, the view perpendicular to the ground plane from the virtual camera can still be obtained if the homography mapping between the image plane and the ground plane is known [20,21].

In the following subsections, a short overview of the homography estimation procedures based on point correspondences and using conic properties is given.

2.2. Homography estimation from point correspondences

In order to estimate the homography, Eq. (3) is rewritten into a special form:

$$\begin{bmatrix} \boldsymbol{p}_w^T & \boldsymbol{0}^T & -x_p \boldsymbol{p}_w^T \\ \boldsymbol{0}^T & \boldsymbol{p}_w^T & -y_p \boldsymbol{p}_w^T \end{bmatrix} \boldsymbol{g} = \boldsymbol{0}, \tag{8}$$

where $\boldsymbol{g}^T = [\boldsymbol{g}_1^T \ \boldsymbol{g}_2^T \ \boldsymbol{g}_3^T]$. Given n point correspondences, by stacking together n equations as (8) a linear system in the form

$$\boldsymbol{\Psi} \boldsymbol{g} = \boldsymbol{0}, \tag{9}$$

is obtained, where $\boldsymbol{\Psi} \in \mathbb{R}^{2n} \times \mathbb{R}^9$ and $\boldsymbol{0}$ is a null vector of length $2n$. The calibration points must not be collinear to avoid ill-conditioning of the system (9). The solution $\boldsymbol{g}$ is defined up to a scale factor, so additional constraint is needed [25]. Imposing the constraint $\boldsymbol{g}^T \boldsymbol{g} = 1$, the solution is known to be the eigenvector of $\boldsymbol{\Psi}^T \boldsymbol{\Psi}$ associated with the smallest eigenvalue. To improve numerical stability of the solution some sort of data normalization should be performed, e.g. as suggested in [26]. According to the noise model a more geometrically meaningful error can be defined, and the solution can be refined through maximum likelihood inference [3].

In the obtained homography matrix, the origin of the world plane may not be where we desire. It is simple to show that the world coordinate frame can be translated and rotated to arbitrary location without repeating the estimation procedure (9). Only one more similarity transform (with constant scale factor) needs to be appended to the right-hand side of the homography $\boldsymbol{G}$ that achieves the desired placement of the world plane coordinate frame — the whole process can be achieved through image interaction.

In a case, when only the relative lengths between the points in world space are known, the homography can be estimated up to the unknown scale factor.

2.3. Homography estimation using conic properties

There are some special properties about the circles (conics) under projective transformation. Two conics always intersect at four complex or real points. Two coplanar circles always intersect at two complex points at infinity $\boldsymbol{p}_{w\{a,b\}}^T = [1 \ \pm i \ 0]$, known as *circular points*. These two circular points lie on the line at infinity $\boldsymbol{l}_{w\infty}^T = [0\ 0\ 1]$ and are transformed into the images of the circular points (ICPs) $\boldsymbol{p}_{pa}$ and $\boldsymbol{p}_{pb}$ that lie on the vanishing line $\boldsymbol{l}_{p\infty}$.

Let us describe how the homography up to similarity $\boldsymbol{H}_a \boldsymbol{H}_p$ can be recovered from the image of the circle $\boldsymbol{C}_p$ and the image of the circle centre $\boldsymbol{p}_{p0}$. To determine the pure perspective transformation $\boldsymbol{H}_p$ one has to find the vanishing line $\boldsymbol{l}_{p\infty}^T = [l_1\ l_2\ l_3]$ (see (4)), which is the image of the line at infinity in the world plane. All the parallel lines in the world plane intersect at some vanishing point in the image (see dashed lines in Fig. 2). Two (or more) sets of parallel lines (the lines in one set are not parallel with the lines in any another set) from a common plane, give two (or more) vanishing points, all lying on a common line — the vanishing line $\boldsymbol{l}_{p\infty}$.

As long as the circle in the world plane is in front of the camera, the circle transforms into an ellipse under projective transformation. It is a well known property of the projective transformation that the origin of the ellipse in the image, which is the image of the circle in the world plane, does not coincide with the image of the origin of that circle. This fact can clearly be observed in Fig. 2. The image of the circle (the ellipse) $\boldsymbol{C}_p$, the image of the circle centre $\boldsymbol{p}_{p0}$ and the vanishing line $\boldsymbol{l}_{p\infty}$ are in the polar relation

$$\boldsymbol{l}_{p\infty} = \boldsymbol{C}_p \boldsymbol{p}_{p0}, \tag{10}$$

which gives us a straight-forward way to calculate the vanishing line (Fig. 2).

The vanishing line $\boldsymbol{l}_{p\infty}$ intersects the image of the circle $\boldsymbol{C}_p$ at two virtual points, ICPs $\boldsymbol{p}_{pa}$ and $\boldsymbol{p}_{pb}$. It can be checked that the ICPs are invariant under the similarity transform. From the ICPs all the parameters of the homography matrix up to similarity $\boldsymbol{H}_a \boldsymbol{H}_p$ can be analytically determined, since the two circular points $\boldsymbol{p}_{w\{a,b\}}$ transform into the ICPs $\boldsymbol{p}_{p\{a,b\}} = [b \pm ia, \ \pm i, \ -\frac{l_1 b}{l_3} \mp \frac{l_1 a + l_2}{l_3}]$.

3. Self calibration from circular motion

The camera calibration procedure described in Section 2.2 requires knowledge of the world points lying on a common plane and the corresponding image points. In this section we present a calibration procedure for estimation of the homography up to similarity that is based on circular motion of a point around the single axis.

Without loss of generality, suppose a camera is observing a point that is rotating in a plane around a single axis. The motion

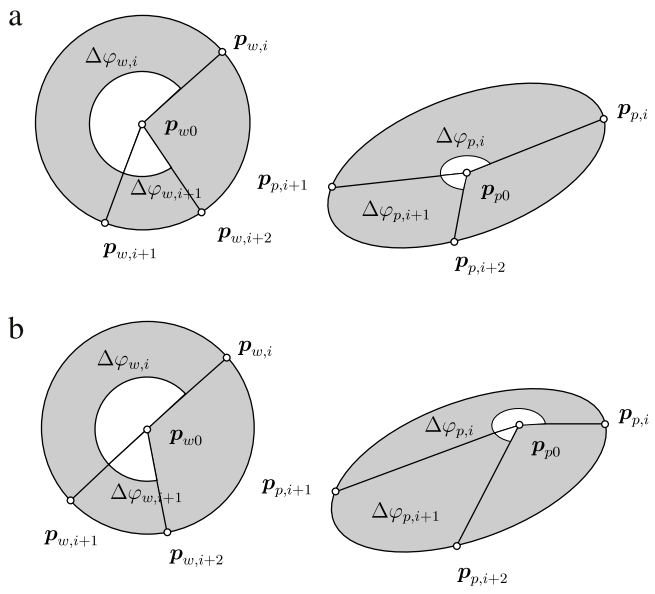

Fig. 3. Two different hypotheses regarding the image of the circle centre (world plane on left and image plane on right) – $\Delta\varphi_{\{p,w\},i} = \varphi_{\{p,w\},i+1} - \varphi_{\{p,w\},i}$.

of the point (x_w, y_w) in the world plane can be described by the following model:

$$x_w(t) = \int_0^t \nu(\tau)\cos(\varphi_w(\tau))\mathrm{d}\tau + x_w(0),$$
$$y_w(t) = \int_0^t \nu(\tau)\sin(\varphi_w(\tau))\mathrm{d}\tau + y_w(0), \tag{11}$$
$$\varphi_w(t) = \int_0^t \omega(\tau)\mathrm{d}\tau + \varphi_w(0),$$

where ν and ω represent the tangential and angular velocity of the point, respectively. Initial conditions define the position and orientation of the origin of the world frame and are usually not known precisely. At this point the initial conditions can all be set to arbitrary values, because, as already mentioned in Section 2.2, the origin of the world plane can be determined after calibration.

Numerical integration of Eqs. (11) introduces drift, which limits the integration time in order to stay within an acceptable error region. Let us set the tangential and angular velocities to constant non-zero value, so in steady-state circular motion of the rotating point should be achieved. One of the advantages of constant velocities is their invariance to delays and elimination of numerical integration. With selection $\nu(t) = \nu = const.$ and $\omega(t) = \omega = const.$, analytical solution for the world coordinates can be obtained from Eq. (11):

$$x_w(t) = \frac{\nu}{\omega}(\sin(\omega t + \varphi_w(0)) - \sin(\varphi_w(0))) + x_w(0),$$
$$y_w(t) = -\frac{\nu}{\omega}(\cos(\omega t + \varphi_w(0)) - \cos(\varphi_w(0))) + y_w(0).$$

Since the initial conditions can be set to arbitrary values, we take the following selection: $x_w(0) = \frac{\nu}{\omega}$, $y_w(0) = 0$ and $\varphi_w(0) = \frac{\pi}{2}$, which yields:

$$x_w(t) = \frac{1}{\kappa}\cos(\omega t) \quad \text{and} \quad y_w(t) = \frac{1}{\kappa}\sin(\omega t). \tag{12}$$

The relation between the angular and tangential velocity defines the curvature of the circular path $\kappa = \frac{\omega}{\nu}$. In order to obtain satisfactory estimation results, the input signals must be carefully chosen to achieve an adequately large radius (small curvature) of the circular path.

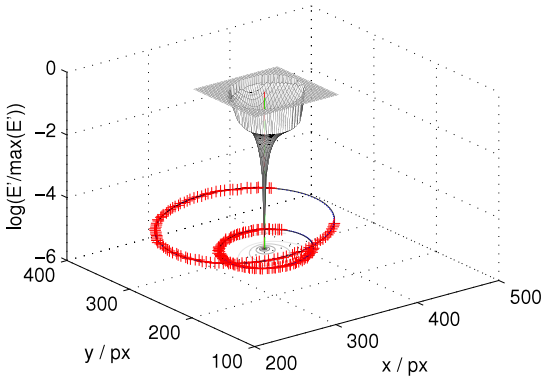

Fig. 4. Cost function for determining the image of the circle centre by Lourakis' method when 80% of the full circle is available.

3.1. Direct method: homography estimation from point correspondences

The homography can be estimated from a set of point correspondences between two planes as described in Section 2.2. In our case, all we need to do is to track the position of the image of the point, which is rotating at constant tangential and angular velocity in the world plane, and take note of time. Then, using the model (12), the world points can be calculated.

This approach requires measurement of the angular velocity of the rotating point. The inaccurate information about the angular velocity causes an error in Eq. (12) due to the wrong estimation of the circular path period. This systematic error can be eliminated by estimating the circle period from the period of the ellipse of the tracked point in the image, since the periods of both ellipsoids should be the same. Therefore, the period can be estimated if the rotating point makes at least one full circle. The error in the tangential velocity is not so crucial, because it only influences the radius of the circular path, in other words, it only influences the size of the world unit vector (part of the similarity transform).

3.2. Lourakis' method: homography estimation from coplanar circles

Lourakis presented the procedure for metric rectification from multiple coplanar circles [10]. The algorithm requires at least two coplanar circles (radius ratio need not be known). Here a short summary of the approach is given. First, ellipses are fitted to all the $n > 1$ images of the circles. Then, a two-step search for the projected circle centre of one of the circles (e.g. the circle i) is carried out. In the first step, a hypothesis regarding the image of the ith circle centre $\boldsymbol{p}_{p0}$ is made somewhere inside the ellipse (the image of the circle). Using the assumed circle centre, the homography that would transform the ellipse into a circle is calculated as described in Section 2.3. In the second step, all the other $n - 1$ ellipses are transformed with the same homography. Then, the shapes of all the transformed ellipses are compared to the shape of a circle by some distance measure e.g. by comparing the semi-major M_j and semi-minor axis m_j of the transformed ellipses:

$$E'(\boldsymbol{p}_{p0}) = \sum_{j=1, j\neq i}^{n} \left| 1 - \left(\frac{m_j}{M_j}\right)^2 \right|. \tag{13}$$

Several hypotheses regarding the image of the circle centre $\boldsymbol{p}_{p0}$ are made by selecting many different points inside the ith ellipse envelope. The homography that transforms all the other ellipses to the most ideal circles (i.e. has the smallest value of the criterion function E') is the solution we are looking for.

The algorithm was designed for static images of circles. However, the method can also be used in the case of in-image tracking

Table 1
Quantitative comparison of different rectification methods.

Method	Requirements	Advantages	Disadvantages
Direct	One set of the image points and corresponding time tuples $\{(\boldsymbol{p}_{pi}, t_i)\}$; known angular velocity ω or at least one full circle.	Closed form solution; computationally fast.	Requires knowledge of the point correspondences and angular velocity.
Lourakis'	At least two sets of the image points $\{\boldsymbol{p}_{pi}\}$ corresponding to two images of the circles or parameters $\boldsymbol{C}_{pi}$ of two images of the circles.	Point correspondences need not be known; more robust than the direct method, since it is based on conics (not points).	Iterative method; computationally intensive in a case when high accuracy is required.
Proposed	One set of the image points and corresponding time tuples $\{(\boldsymbol{p}_{pi}, t_i)\}$	Only a single circle is required; the circle need not be a complete full circle; point correspondences need not be known; angular velocity is also estimated.	Iterative method; computationally intensive in a case when high accuracy is required.

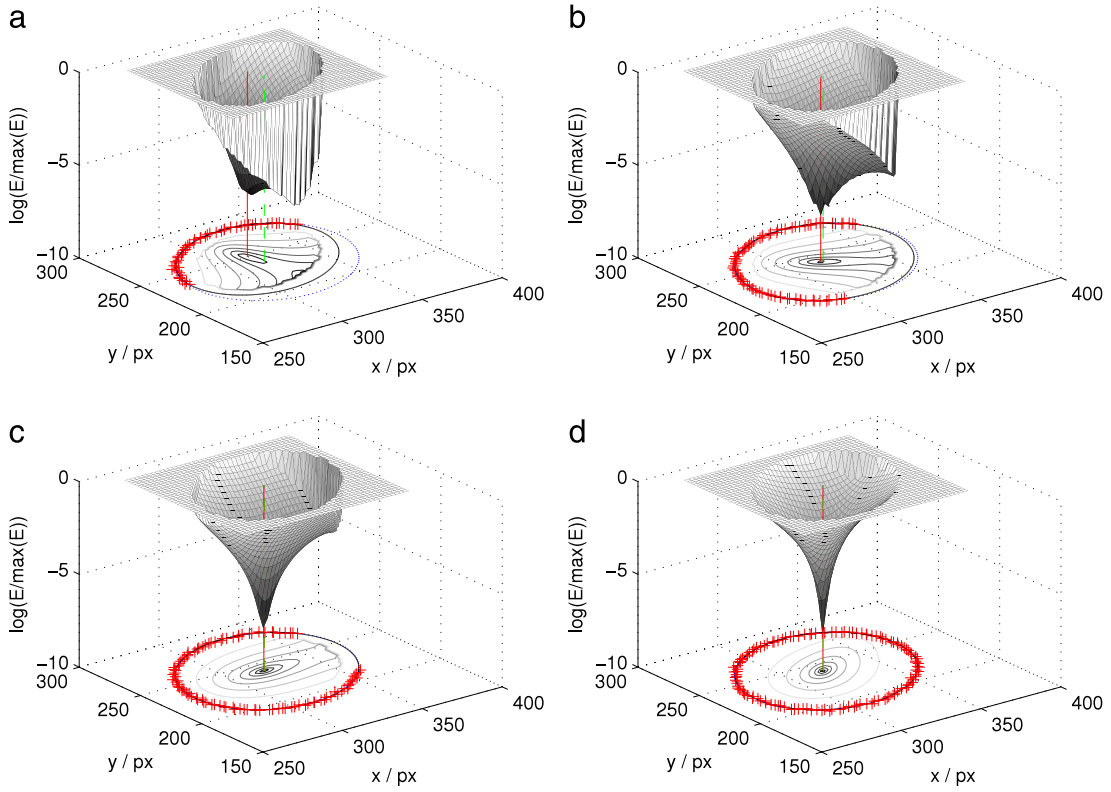

Fig. 5. Cost functions for determining the image of the circle centre by the proposed approach when (a) 40%, (b) 60%, (c) 80% and (d) 100% of the full circle is available, respectively.

of several points that are all rotating in the same plane. In such a case, one advantage of the algorithm is that it does not require the knowledge about the angular velocity and time (the angles around the circle origin). Metric rectification is based on conic features that can normally be determined with higher accuracy than point features. To achieve an adequate accuracy and avoid local minima problems the search area must be partitioned into small enough regions, but that increases the time it takes to find the minimum.

3.3. Proposed approach: homography estimation from circular motion

Suppose, the camera is observing an object that is rotating at constant angular velocity around a single axis in some world plane. The image tracking algorithm is following a single point in the rotating object. As a result of the tracking a set of N tracked points in the image frame with the corresponding times of observation $\{(\boldsymbol{p}_{pi}, t_i)\}_{i=1,2,\ldots,N}$ is obtained. If the observed point is always in front of the camera plane, the set of points from a circle in the world frame form an ellipse in the image frame. Our approach then goes as follows. To the set of the image points $\{\boldsymbol{p}_{pi}\}_{i=1,2,\ldots,N}$ the ellipse $\boldsymbol{C}_p$ is fitted. There are many methods for conic (ellipse) fitting [27,28]. Since we known the image of a circle is an ellipse it is the best to use a method that takes this assumption into account (e.g. see implementation [29]). The homography up to similarity is then uniquely determined by the image of the circle centre. As opposed to Lourakis' method, who uses the images of the another coplanar circle to find the image of the circle centre, the proposed approach makes use of the time series $\{t_i\}_{i=1,2,\ldots,N}$ as follows. The basic idea of the approach is that the angle φ_w around the circle centre is considered to be proportional to the time of observation t, since the rotating point is assumed to be rotating at constant angular velocity.

The procedure for plane rectification can be summarized in the following steps:

1. Fit the ellipse $\boldsymbol{C}_p$ to the set of points $\{\boldsymbol{p}_{pi}\}_{i=1,2,\ldots,N}$.
2. Partition the area inside the ellipse envelope into a grid.
3. For every point in the grid do:
   (a) Mark the selected point as $\boldsymbol{p}_{p0}^T = [x_{p0}\ y_{p0}\ 1]$.
   (b) Determine the homography matrix $\boldsymbol{H}$ that transforms the ellipse $\boldsymbol{C}_p$ into a circle and the point $\boldsymbol{p}_{p0}$ into the centre of that circle as described in Section 2.3.
   (c) Calculate the set of angles $\{\varphi_{pi} = \arg(\boldsymbol{p}_{pi} - \boldsymbol{p}_{p0})\}_{i=1,2,\ldots,N}$ and insert them into Eq. (7) to obtain the set of angles $\{\varphi_{wi}\}_{i=1,2,\ldots,N}$.

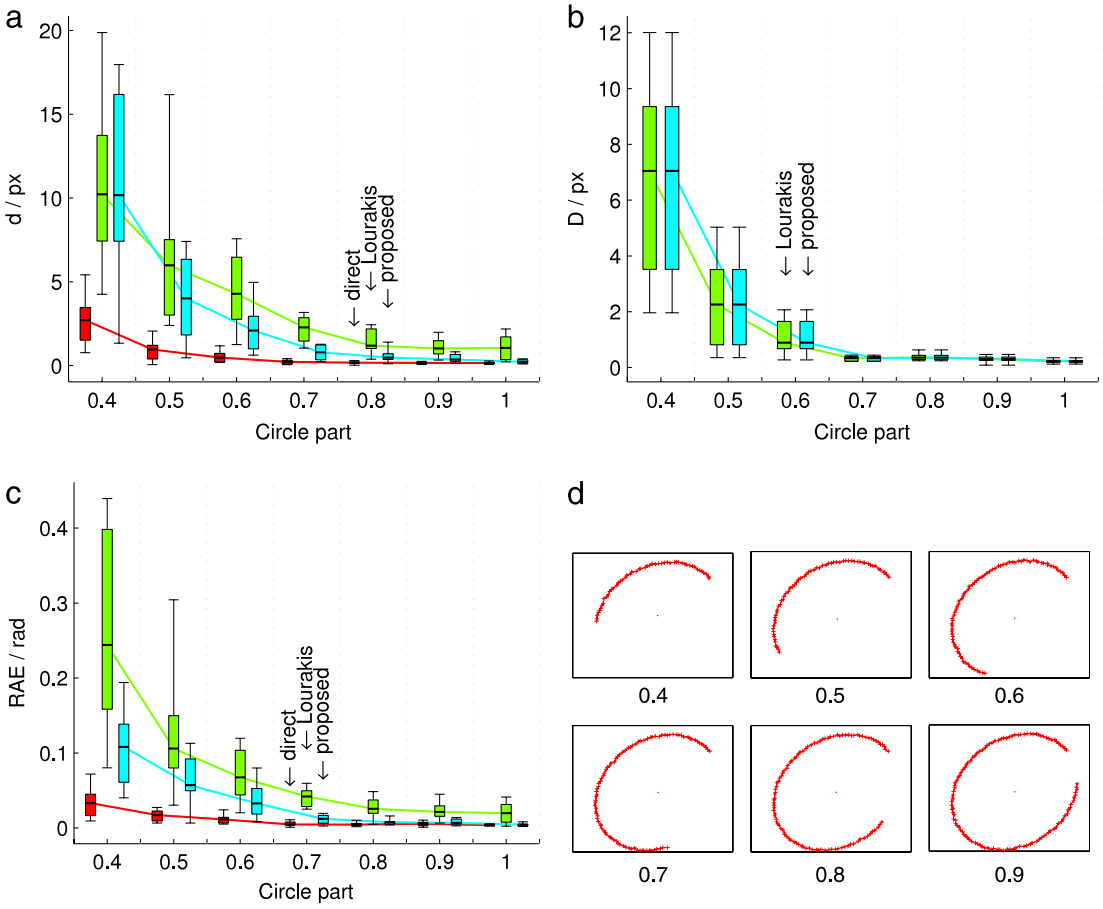

Fig. 6. The influence of the part of the circle available to (a) the error in estimation of the image of the circle centre, (b) the ellipse fitting error and (c) the rectification absolute error RAE. (d) The images of data at different part of the available circle.

(d) Find the parameters ω and ϕ using the least squares method that minimize the cost function

$$E(\boldsymbol{p}_{p0}) = \min_{\omega,\phi} \sum_{i=1}^{N} \varphi_{wi} - \omega t_i - \phi, \tag{14}$$

where ϕ is a scalar that determines the initial angle in the world plane, and ω is the unknown angular velocity.

4. Choose the $\boldsymbol{p}_{p0}$ as the image of the circle centre, ω as the angular velocity of the rotating object and $\boldsymbol{H}$ as the homography that has the minimum cost function E among all the points from the search area.

Two different hypotheses regarding the image of the circle centre can be seen in Fig. 3. In a case of the true image of the circle centre, the angles in the world plane are proportional to the measured time. The method can give the smallest value of the cost function E when the image of the circle centre is near the ellipse envelope, even if the true circle centre does not lie there. The problem can be avoided by defining some forbidden margin around the ellipse envelope where the search for the image of the circle centre should not be carried out.

The proposed method requires some encirclement of only a single point in the world plane. The most important advantages of the method over the direct method presented in Section 3.1 are: the homography up to similarity can be estimated even when the data from only a part of the circle is available; the angular velocity is also estimated during the process. The approach is quite computationally intensive if we want to achieve satisfactory accuracy, since we need to search the whole area inside the ellipse envelope. The computational intensity is in the same time range as in Lourakis' approach. However, the computational burden can be reduced by starting with a very rough mesh, and then making several refinements around the minimum. The advantage over Lourakis' method given in Section 3.2 is that the proposed method only require one circle. The quantitative comparison of all the presented methods is summarized in Table 1.

The proposed method is also applicable in a case of a static scene (no rotations) where a circle is available with some points for which the angle between them is known, but the image of the circle centre cannot be determined from the image.

4. Experiments

4.1. Synthetic data

We validated all three methods for estimation of the homography up to similarity $\boldsymbol{H}_a\boldsymbol{H}_p$ on synthetic data. We simulated the motion of two points rotating in the same plane. That resulted in two circular trajectories: a circle with the radius $r_1 = 0.2$ m rotating at the angular velocity $\omega_1 = 0.5$ rad/s around the ground frame origin and a circle with the radius $r_2 = 0.4$ m rotating at the angular velocity $\omega_2 = 0.5$ rad/s around the point (0.2 m, 0.2 m) in the ground plane. The configuration of the projection plane with respect to the ground plane was selected to be as given by the following homography matrix:

$$\boldsymbol{G} = \begin{bmatrix} 0.4643 & -0.1739 & 0.5317 \\ 0.3255 & 0.4545 & 0.3987 \\ 0 & 0.0003 & 0.0017 \end{bmatrix}. \tag{15}$$

The circular trajectories were sampled at sample time $T_s = 0.1$ s.

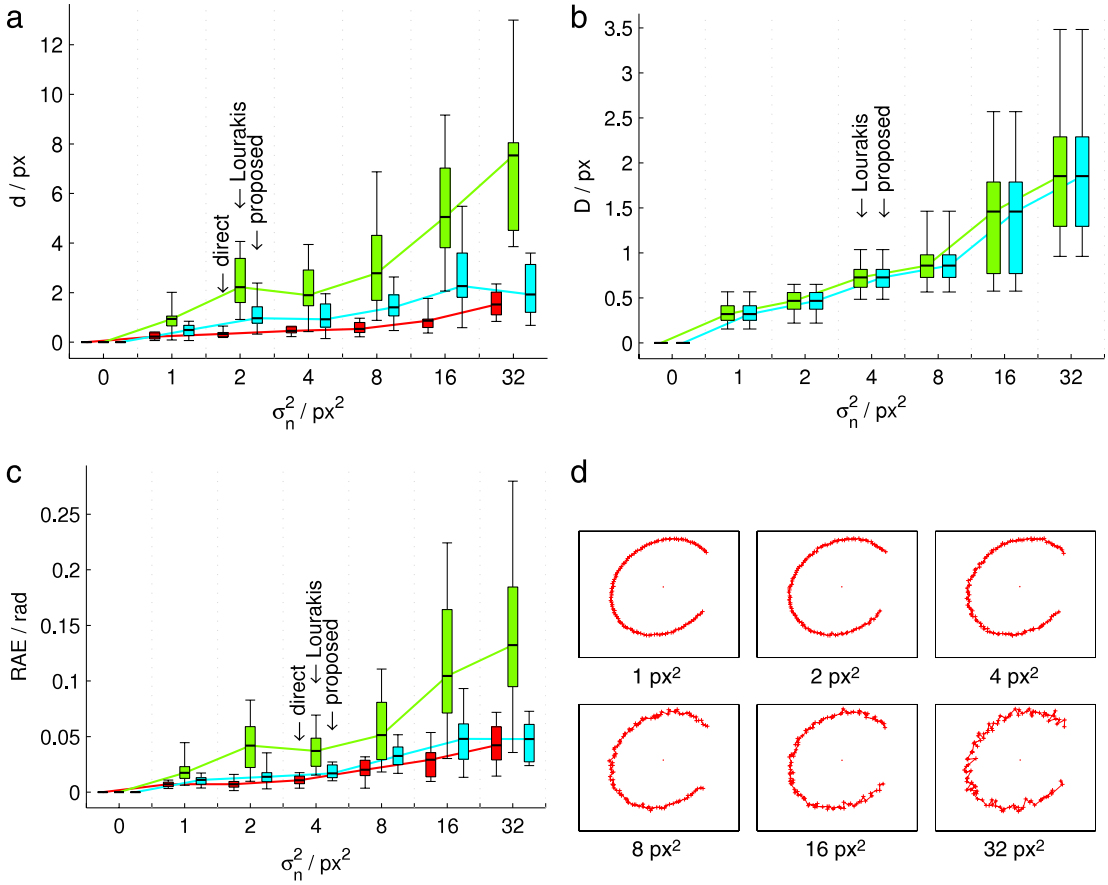

Fig. 7. The influence of the noise in the measurement of the points in the image frame to (a) the error in estimation of the image of the circle centre, (b) the ellipse fitting error and (c) the rectification absolute error RAE. (d) The images of the data at various noise levels.

We assumed that the time of observation is only 80% of the time it takes to complete one full circle, and Gaussian white noise with the variance $\sigma_n^2 = 1$ px^2 is added to the measured points in the image frame. Under given conditions, Figs. 4 and 5c show the cost functions for estimation of the image of the circle centre by Lourakis' method and the proposed method. The search area for the image of the circle centre was partitioned into 40×40 search grid and the result around the minimum was refined three times. All the cost functions are plotted in logarithmic scale to improve visibility of the minimum. The direct approach is not included in the comparison of the cost functions, since it does not require to evaluate the image of the circle centre with a cost function. Fig. 5 shows cost functions of the proposed method for different durations of observation (less or equal to the time it takes to make one full circle).

All the calibration methods were evaluated for robustness with respect to different disturbances and non-ideal conditions. In the direct method, we assumed that the true angular velocity ω was known, although in the real world this is usually not the case. The calibration procedures were repeated several times to ensure statistically accurate results (ten times in our case). To compare the performance of all the methods, several criterion functions were defined. To evaluate the homography up to similarity by Lourakis' and the proposed method an accurate estimation of the image of the circle centre and an accurate fit of the ellipse to the image of the circle is needed. The error in estimation of the image of the circle centre was defined as follows:

$$d = \sqrt{(\hat{\mathbf{p}}_{p0} - \boldsymbol{p}_{p0})^T (\hat{\mathbf{p}}_{p0} - \boldsymbol{p}_{p0})}\,, \tag{16}$$

where $\hat{\mathbf{p}}_{p0}$ is the estimated image of circle centre and $\boldsymbol{p}_{p0}$ is the true image of the circle centre. The accuracy of the ellipse fit was evaluated using the following error function:

$$D = \frac{1}{N} \sum_{j=1}^{N} \sqrt{(\hat{\mathbf{p}}_{p,j} - \boldsymbol{p}_{p,j})^T (\hat{\mathbf{p}}_{p,j} - \boldsymbol{p}_{p,j})}\,, \tag{17}$$

where the point $\boldsymbol{p}_{p,j}$ represents a point on the envelope of the ellipse that is estimated by the point $\hat{\mathbf{p}}_{p,j}$ in a way that both points share the same angle around the ellipse centre. In order to achieve satisfactory precision, the number of points N where the mismatch between the ellipses is evaluated should be high and the points should be distributed uniformly around the centre of the reference ellipse (in our case $N = 1000$). Furthermore, an additional criterion for evaluation of the rectification performance was defined that is based on orthogonality of the lines:

$$RAE = \frac{1}{4} \sum_{j=1}^{4} \left| \frac{\pi}{2} - \gamma_j \right|, \tag{18}$$

where γ_j is the angle between the rectified images of the two lines that are perpendicular in the world plane. In the criterion (18) four perpendicular lines are considered that form a square and cross at four points around which the four angles γ_j, $j \in \{1, 2, 3, 4\}$, are calculated. In an ideal case the RAE criterion (18) should be zero. Since the RAE directly evaluates the performance of the image rectification, it is considered to be the most relevant error criterion, but the other two presented errors, (16) and (17), can give some additional insight into estimation performance. In short, the error in homography estimation can occur due to bad ellipse fitting, or else the error is due to wrong circle centre estimation.

Fig. 6a shows the error in estimation of the image of the circle centre for all three methods with respect to the part of the full

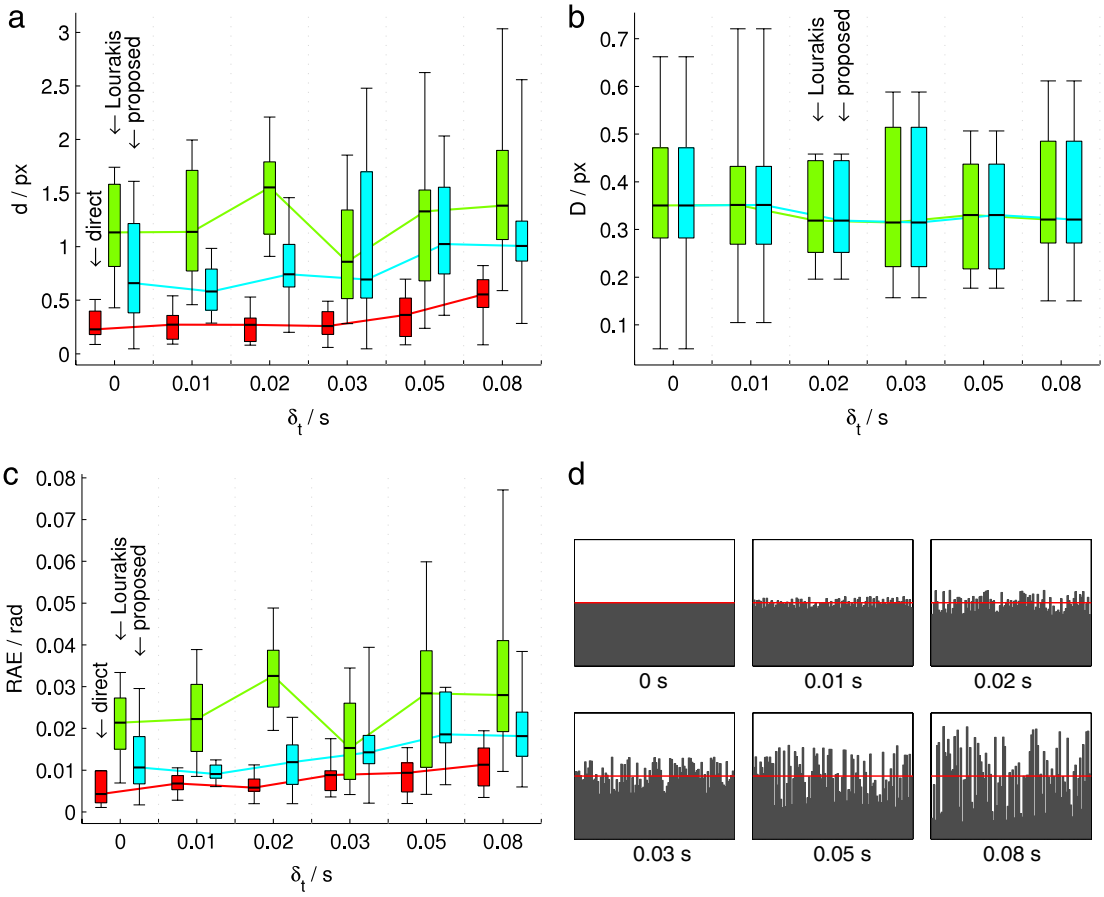

Fig. 8. The influence of the noise in the measurement of the time to (a) the error in estimation of the image of the circle centre, (b) the ellipse fitting error and (c) the rectification absolute error RAE. (d) The various levels of uniformly distributed noise in the measurement of the time.

circle available. For the same case, Fig. 6b shows the error in ellipse fitting, and Fig. 6c shows the absolute rectification error RAE. In all the figures the mean error from all the repetitions of the same experiment is shown, together with the minimum and maximum error, and the range in which half of the measurements can be found.

Fig. 7 presents the results of robustness to the noise with the variance σ_n^2 in the measurement of the points in the image frame. We assumed that only 80% of the full circle was available for calibration.

The methods were also evaluated for performance to noise in the measurement of the time with a uniform distribution of the noise with the amplitude δ_t (Fig. 8). We again assumed that only 80% of the full circle is available, and that the measurement of the points in the image frame is disturbed by Gaussian white noise with variance $\sigma_n^2 = 1\ \text{px}^2$.

The performance of the estimation approaches was also tested for susceptibility to the inclination ψ of the projection plane with respect to the ground plane. The same assumptions as presented in the previous paragraph were made. Since every inclination of the camera with respect to the ground plane is represented by different homography, a set of these homographies can be used to estimate the intrinsic camera parameters. The intrinsic parameters of the camera used in the experiments were:

$$x_{pc} = 320, \quad y_{pc} = 240, \quad \alpha = \beta = 1000, \quad \gamma = 50. \tag{19}$$

Taking all the estimated homographies at different inclinations, the following intrinsic camera parameters were estimated using the approach described in [3]:

$$\hat{x}_{pc} = 311.2554, \quad \hat{y}_{pc} = 262.8430,$$
$$\hat{\alpha} = 1009.4, \quad \hat{\beta} = 1009.7, \quad \hat{\gamma} = 54.9693. \tag{20}$$

4.2. Real data

We made real experiments on a two wheeled differentially driven mobile system normally used in the FIRA MiroSot robot soccer small league. The mobile system was marked with a colour badge to be easily tracked by an overhead camera [24]. We used an IEEE-1394 digital colour camera with the resolution of 640 × 480 px^2. The camera was placed at an inclined angle with respect to the ground plane. Constant control velocities were sent to the robot ($v_c = 0.4$ m/s and $\omega_c = 2$ rad/s). At each time step ($T_s = 0.1$ s) we measured the position of the robot in the image frame and the image acquisition time. The measured data in the image frame for four circles at different locations is shown in Fig. 10.

All the presented calibration approaches were experimentally tested on the data of the circles one to four. In the case of Lourakis' method, the other circles of the selected one were used for the calculation of the cost function (14). In Table 2, estimations of the images of the circle centres are gathered. Figs. 11a–c show the rectified images by all three methods when the data of the first circle is used. The orthogonal lines of the soccer field lying in the ground plane should appear orthogonal in the rectified images, so we can visually evaluate the accuracy of the calibration methods by observing the transformed images.

5. Discussion

Both cost functions in Figs. 4 and 5c have strong minimum at the image of the circle centre. As it can be observed in Fig. 5, the cost function of the proposed method wraps down near ellipse boundary as smaller part of the full circle is available. This can lead

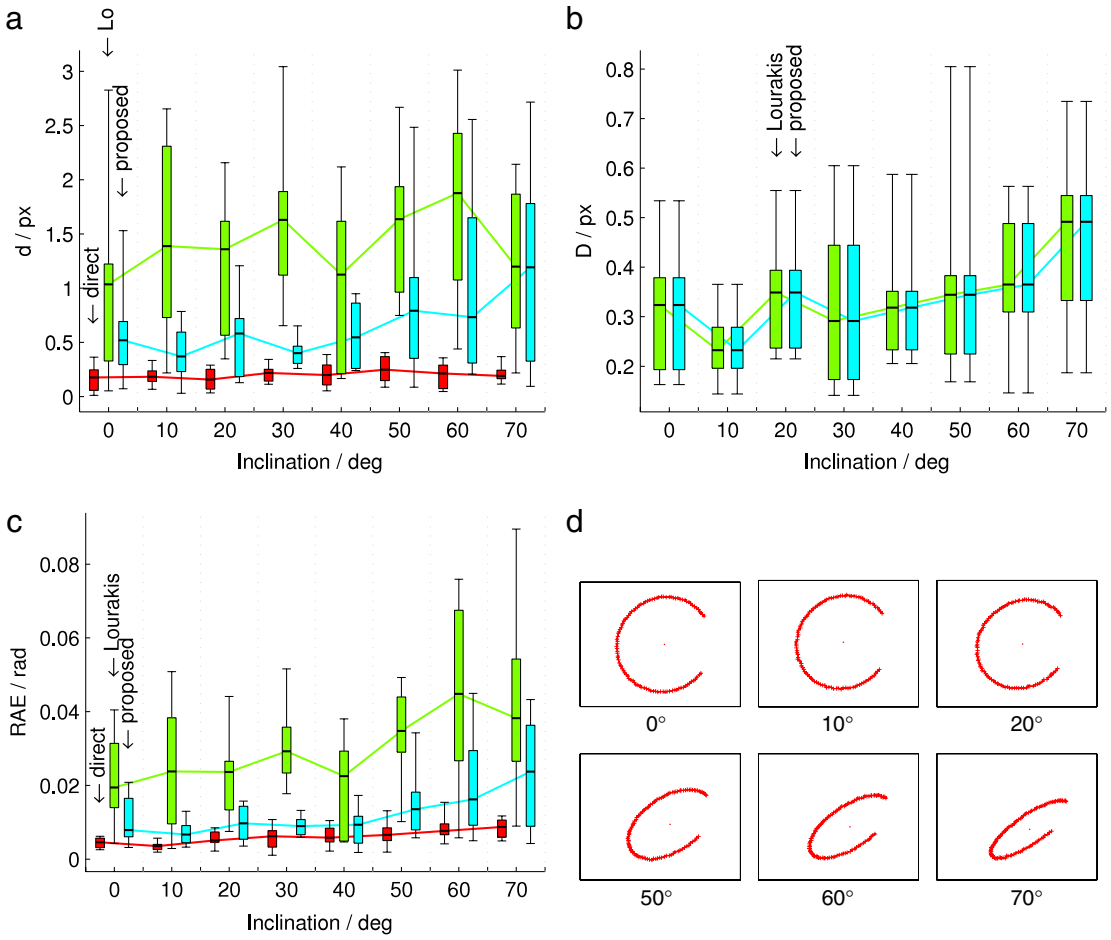

Fig. 9. The influence of the inclination of the projection plane with respect to the ground plane to (a) the error in estimation of the image of the circle centre, (b) the ellipse fitting error and (c) the rectification absolute error RAE. (d) The images of the circle at various inclinations with respect to the ground plane.

Table 2
Comparison of estimation of the image of the circle centre for all the calibration methods on real data.

Method	Circle	Circle 1	Circle 2	Circle 3	Circle 4
Direct	$(x_{p0}, y_{p0})/px$	(303.522, 276.54)	(441.901, 271.669)	(397.937, 212.223)	(213.39, 318.794)
Lourakis	$(x_{p0}, y_{p0})/px$	(304.512, 274.62)	(438.675, 270.75)	(397.692, 213.389)	(210.997, 317.479)
Proposed	$(x_{p0}, y_{p0})/px$	(303.935, 274.511)	(438.954, 270.509)	(397.884, 213.273)	(210.522, 317.299)
	ω/s^{-1}	2.045	2.050	2.046	2.053
Direct*	$(x_{p0}, y_{p0})/px$	(303.906, 274.517)	(439.007, 270.512)	(397.919, 213.256)	(210.5, 317.311)

to wrong estimation of the circle centre. This problem is avoided when a large-enough part of the circle is available. Another thing to mention that applies to Lourakis' and the proposed method is that sensitivity of the method used for fitting an ellipse [29] greatly increases when only a small part of the ellipse envelope is available. In Fig. 5a, where measurements from only 40% of the full circle are available, it can be seen that the ellipse (solid line) fitted to the measured points (positive-sign markers) does not match accurately the true image of the circle (dotted line), and this is also the reason that the estimated image of the circle centre does not coincide with the true value.

As smaller and smaller part of the complete circle is available the error in estimation of the image of the circle centre increases in all the methods. The error of the direct method can be seen as the reference error, but should be noted that we assumed that the angular velocity was known a-priori. The error in estimation of the image of the circle centre of the other two methods converges to the error of the direct method when the circle part limits towards the full circle. Because the direct method does not need ellipse fitting, only the other two methods were compared in Fig. 6b, where the results for both methods are the same, since the same ellipse fitting algorithm was used in both methods. As expected, the ellipse fitting is better when the image of a larger part of the full circle is available.

As expected, when the noise level in the measured points increases, the ellipse fitting error also increases. In Lourakis' and the proposed method the estimation of the image of the circle centre is dependent on the accuracy of the ellipse fit, so the error in the estimation of the circle centre is also expected to increase with the noise level, and this can be observed in Fig. 7. The RAE measure confirms that the proposed estimation procedure gives more accurate results than Lourakis' method and the performance of the proposed approach is better than the Lourakis method and close to the direct method.

The noise in the measurement of the time influences the estimation of the image of the circle centre only in the proposed and the direct method, which is expected, since Lourakis' approach does not require measurement of time (but it requires two or more

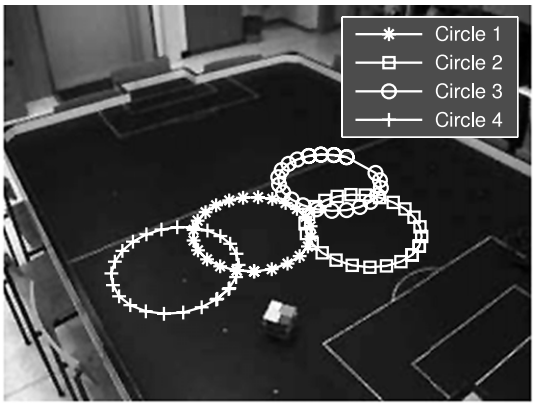

Fig. 10. Real camera view and measurements of the four coplanar circular trajectories.

circles). Nevertheless, the influence of the noisy measurements of time to the accuracy of the estimation is significantly smaller than with respect to the noise in the image points and circle part.

The results in Fig. 9 show some susceptibility of all the methods to the inclination. Again, the proposed method gives satisfactory results. Even though the homographies are estimated with satisfactory precision, the camera intrinsic parameters estimated from multiple homographies (obtained at different inclinations) may not give satisfactory results, since the approach used (described in [3]) seems to be quite susceptible to noise. However, the camera intrinsic parameters can be obtained from multiple homographies. Since the same data, as used in Fig. 9, could be generated with rotating camera around a single axis with tracking of an off-axis point, the proposed approach could be used to estimate the intrinsic parameters of a camera mounted at the end-effector of a robotic manipulator with circular joints. In a case one of the joint of the robotic arm manipulator is set to rotate at constant angular velocity and the camera is tracking a single point, a single homography can be estimated. Afterwards some of the other joints of the robotic arm manipulator can be reconfigured to achieve different inclination of the camera with respect to the axis of rotation. In this way a set of homographies is obtained that can be used in estimation of the camera intrinsic parameters.

Regarding the real data (Fig. 10), the direct method does not give as good results as Lourakis' and the proposed method. That is due to the fact that the angular velocity is not measured and therefore not known exactly. From Table 2 we can see that the estimated angular velocity by the proposed method is not equal to the angular velocity control command $\omega_c = 2$ rad/s. From a quick look at the estimated images of the circle centres, the difference may not seem significant. Using the angular velocity estimated by the proposed method, we repeated the estimation of the homography with the direct method (denoted as direct* in Table 2). As a result, the rectified image in Fig. 11d gives satisfactory results. We can conclude that the direct method is indeed very susceptible to the error in the angular velocity, and that the proposed method can solve the metric rectification problem.

The computational burden of the proposed method and Lourakis' method is in the same time range (several seconds in the proposed implementation on a contemporary computer), and it is significantly more time-consuming as the direct method (hundreds of milliseconds). As already mentioned, the time consumption of the proposed and Lourakis' method is dependent on the resolution of the search area. The search for the image of the circle centre was carried out in a way that refines the search grid several times (three times in the proposed case). In this way, we reduced the search time from several tens of seconds to only several seconds, but were able to achieve the same accuracy. In the proposed method, the search algorithm for the optimum solution could be speeded-up even more by using some additional optimization techniques. However, the time consumption is not a significant drawback of the method, since calibration algorithms normally do not need to be executed in real time.

6. Conclusion

Several methods for estimation of the homography up to similarity from the circular motion were presented. The study was focused on a case when the camera is observing and tracking a single point on an object that is rotating at constant angular velocity around a fixed axis. Since the direct method and the approach proposed by Lourakis may not give satisfactory results for the considered case in the presence of disturbances and non-ideal conditions, a new method for estimation of the homography up to similarity was developed that is specialized for calibration from circular motion around a single axis. The main drawback of the direct method is that it requires a-priori knowledge of the angular velocity. The method proposed by Lourakis requires at least two coplanar circles, and these may be hard to generate in some visual servoing configurations. The proposed method is well suited for use in several visual servoing applications, since the calibration process can be achieved without special preparation of the environment. The main advantages of the proposed method are that it estimates the angular velocity and that it only requires a single circle for the estimation. Another benefit of the proposed method is that the estimation of the homography is based only on the measurements obtained in the image.

The presented method was experimentally validated and compared to the other two methods. The results prove that the proposed method was able to achieve satisfactory accuracy in different configurations and even in the presence of disturbances. The experiments made on synthetic data also showed that it is possible to obtain the camera intrinsic parameters from multiple homographies. The real experiments, made on the mobile system normally used in the robot soccer small league, demonstrated how the proposed method could be used to eliminate the perspective projection.

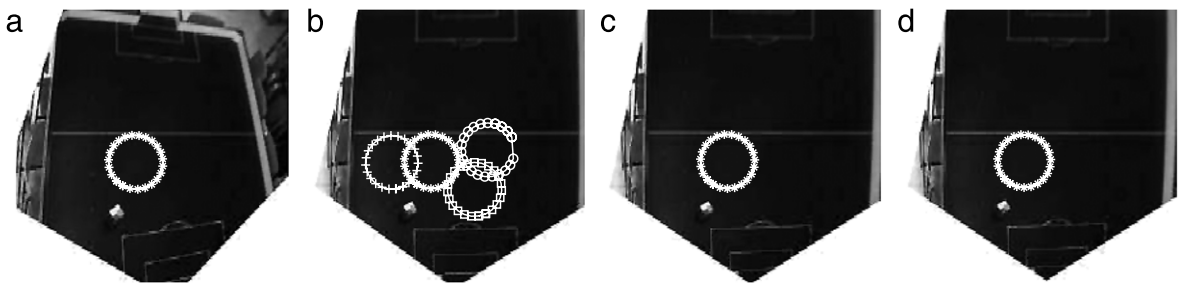

Fig. 11. Rectified images of the image in Fig. 10 using the data of the circle 1 with (a) the direct method, (b) Lourakis' method (the other circles are used for estimation of the first circle centre), (c) proposed method and (d) the direct method with angular velocity estimated by the proposed method.

References

[1] R. Hartley, A. Zisserman, Multiple View Geometry, second ed., Cambridge University Press, New York, USA, 2004.
[2] R.Y. Tsai, A versatile camera calibration technique for high-accuracy 3D machine vision metrology using off-the-shelf TV cameras and lenses, IEEE J. Robot. Autom. 3 (4) (1987) 323–344. http://dx.doi.org/10.1109/JRA.1987.1087109.
[3] Z. Zhang, A flexible new technique for camera calibration, IEEE Trans. Pattern Anal. Mach. Intell. 22 (11) (2000) 1330–1334.
[4] C. Hughes, P. Denny, M. Glavin, E. Jones, Equidistant fish-eye calibration and rectification by vanishing point extraction, IEEE Trans. Pattern Anal. Mach. Intell. 32 (12) (2010) 2289–2296. http://dx.doi.org/10.1109/TPAMI.2010.159.
[5] J. Heikkila, Geometric camera calibration using circular control points, IEEE Trans. Pattern Anal. Mach. Intell. 22 (10) (2000) 1066–1077. http://dx.doi.org/10.1109/34.879788.
[6] A. Sugimoto, A linear algorithm for computing the homography from conics in correspondence, J. Math. Imaging Vision 13 (2) (2000) 115–130.
[7] P.K. Mudigonda, C.V. Jawahar, P.J. Narayanan, Geometric structure computation from conics, in: Proc. Indian Conf. Computer Vison, Graphics and Image Processing, ICVGIP, 2004, pp. 9–14.
[8] H. H. Ip, Y. Chen, Planar rectification by solving the intersection of two circles under 2D homography, Pattern Recognit. 38 (7) (2005) 1117–1120. http://dx.doi.org/10.1016/j.patcog.2004.12.004.
[9] Y. Wu, X. Li, F. Wu, Z. Hu, Coplanar circles, quasi-affine invariance and calibration, Image Vis. Comput. 24 (4) (2006) 319–326. http://dx.doi.org/10.1016/j.imavis.2005.11.008.
[10] M. I. Lourakis, Plane metric rectification from a single view of multiple coplanar circles, in: 2009 16th IEEE International Conference on Image Processing, ICIP, IEEE, 2009, pp. 509–512. http://dx.doi.org/10.1109/ICIP.2009.5413978.
[11] D. C. Brown, Close-range camera calibration, Photogramm. Eng. 37 (8) (1971) 855–866.
[12] X. Meng, Z. Hu, A new easy camera calibration technique based on circular points, Pattern Recognit. 36 (5) (2003) 1155–1164. http://dx.doi.org/10.1016/S0031-3203(02)00225-X.
[13] J.-S. Kim, P. Gurdjos, I.-S. Kweon, Geometric and algebraic constraints of projected concentric circles and their applications to camera calibration, IEEE Trans. Pattern Anal. Mach. Intell. 27 (4) (2005) 637–642. http://dx.doi.org/10.1109/TPAMI.2005.80.
[14] K. Wong, P. Mendonca, R. Cipolla, Camera calibration from surfaces of revolution, IEEE Trans. Pattern Anal. Mach. Intell. 25 (2) (2003) 147–161. http://dx.doi.org/10.1109/TPAMI.2003.1177148.
[15] A. W. Fitzgibbon, G. Cross, A. Zisserman, Automatic 3D model construction for turn-table sequences, in: R. Koch, L. Gool (Eds.), 3D Structure from Multiple Images of Large-Scale Environments, in: Lecture Notes in Computer Science, Springer, Berlin Heidelberg, 1998, pp. 155–170. http://dx.doi.org/10.1007/3-540-49437-5_11.
[16] G. Jiang, L. Quan, H.-T. Tsui, Circular motion geometry using minimal data, IEEE Trans. Pattern Anal. Mach. Intell. 26 (6) (2004) 721–731. http://dx.doi.org/10.1109/TPAMI.2004.4.
[17] E. Malis, M. Vargas, Deeper Understanding of the Homography Decomposition for Vision-based Control, Tech. Rep. INRIA, Nice, France, 2007.
[18] S. Lumbar, G. Dolanc, D. Vrečko, S. Strmčnik, D. Matko, Automatic guidance of an aircraft using predictive control in a visual servoing scheme, in: 18th IFAC Symposium on Automatic Control in Aerospace, ACA, Nara, Japan, 2010, p. 6.
[19] M. Bošnak, D. Matko, S. Blažič, Quadrocopter hovering using position-estimation information from inertial sensors and a high-delay video system, J. Intell. Robot. Syst. 67 (1) (2011) 43–60. http://dx.doi.org/10.1007/s10846-011-9646-5.
[20] R.S. Rao, V. Kumar, C.J. Taylor, Planning and control of mobile robots in image space from overhead cameras, in: Proceedings of the 2005 IEEE International Conference on Robotics and Automation, no. April, IEEE, Barcelona, Spain, 2005, pp. 2185–2190. http://dx.doi.org/10.1109/ROBOT.2005.1570437.
[21] A. Zdešar, I. Škrjanc, G. Klančar, Visual trajectory-tracking model-based control for mobile robots, Int. J. Adv. Robotic Syst. 10 (2013) 1. http://dx.doi.org/10.5772/56757.
[22] G. López-Nicolás, C. Sagüés, J. Guerrero, Homography-based visual control of nonholonomic vehicles, in: IEEE International Conference on Robotics and Automation, no. April, IEEE, Roma, Italy, 2007, pp. 1703–1708.
[23] D. Forsyth, J. Ponce, Computer Vision: A Modern Approach, Illustrate Edition, Prentice Hall, 2003.
[24] G. Klančar, M. Kristan, S. Kovačič, O. Orqueda, Robust and efficient vision system for group of cooperating mobile robots with application to soccer robots, ISA Trans. 43 (3) (2004) 329–342.
[25] J. Heikkila, O. Silven, A four-step camera calibration procedure with implicit image correction, in: Proceedings of IEEE Computer Society Conference on Computer Vision and Pattern Recognition, IEEE Comput. Soc., 1997, pp. 1106–1112. http://dx.doi.org/10.1109/CVPR.1997.609468.
[26] R. I. Hartley, In defence of the 8-point algorithm, in: IEEE International Conference on Computer Vision, IEEE, 1995, pp. 1064–1070. http://dx.doi.org/10.1109/ICCV.1995.466816.
[27] Z. Zhang, Parameter estimation techniques: a tutorial with application to conic fitting, Image Vision Comput. 15 (1) (1997) 59–76.
[28] A. Fitzgibbon, M. Pilu, R. B. Fisher, Direct least square fitting of ellipses, IEEE Trans. Pattern Anal. Mach. Intell. 21 (5) (1999) 476–480. http://dx.doi.org/10.1109/34.765658.
[29] N. Chernov, Ellipse fit (direct method), 2009. http://www.mathworks.com/matlabcentral/fileexchange/22684-ellipse-fit-direct-method.

Andrej Zdešar received the B.Sc. degree in 2010 from the Faculty of Electrical Engineering, University of Ljubljana, Slovenia, where he is currently employed in the framework of the national young researchers scheme. His research interests are in the area of visual control, machine vision and autonomous mobile systems.

Igor Škrjanc received the B.Sc., the M.Sc. and the Ph.D. degrees in Electrical Engineering, from the Faculty of Electrical and Computer Engineering, University of Ljubljana, Slovenia, in 1988, 1991 and 1996, respectively. His main research interests are intelligent, predictive control systems and autonomous mobile systems. In 2007 he received the highest research award of the University of Ljubljana, Faculty of Electrical Engineering, and in 2008, the highest award of the Republic of Slovenia for Scientific and Research Achievements, Zois award for outstanding research results in the field of intelligent control. He also received the Humboldt Research Fellowship for Experienced Researchers for the period between 2009 and 2011. Currently, he is a professor for Automatic Control at the Faculty of Electrical Engineering and the head of the research program Modelling, Simulation and Control.

Gregor Klančar received the B.Sc. and Ph.D. degrees in 1999, and 2003, respectively, from the Faculty of Electrical Engineering, University of Ljubljana, Slovenia. His research interests are in the area of fault diagnosis methods, multiple vehicle coordinated control and mobile robotics. Currently, he is an associate professor at the Faculty of Electrical Engineering.